Performance Analysis of the Clutter Map CFAR Detector with Noncoherent Integration

by Chang-Joo Kim
Hyuck-Jae Lee

Nitzberg has analyzed the detection performance of the clutter map constant false alarm rate (CFAR) detector using single pulse. In this paper, we extend the detection analysis to the clutter map CFAR detector that employs M-pulse noncoherent integration. Detection and false alarm probabilities for Swerling target models are derived. The analytical results show that the larger the number of integrated pulses M, the higher the detection probability. On the other hand, the analytical results for Swerling target models show that the detection performance of the completely decorrelated target signal is better than that of the completely correlated target.

I. Introduction

Since the background level is unknown and time-varying at any given location, the radar detector with a fixed threshold can not be applied to the radar returns if one wants to control the false alarm rate. The *constant false alarm rate* (CFAR) detection technique is employed to control the false alarm rate, which estimates the background clutter-plus-noise level and sets a threshold adaptively based on the local information of clutter-plus-noise level. The objective of the CFAR design is to provide a detection threshold that is relatively immune to variations of the background clutter-plus-noise level and to allow target detection with a CFAR.

There are two methods to achieve CFAR: one is to use the sliding window technique and the other is to use a clutter map. As far as the radar detection using sliding window technique is concerned, a lot of work has been done. In the conventional *cell-averaging* (CA) CFAR detector [1], the background clutter-plus-noise level is estimated by averaging the outputs of the neighboring resolution cells (range and/or Doppler). This method may be used if the statistics of the background level is homogeneous. However, most CFAR processors using this technique can not

maintain the optimal performance when homogeneous assumption is violated. For the latter, the estimate of background level is obtained by averaging over several scans. This technique may require long term storage of each of the cells used to get the estimate of background level. In order to reduce the memory size, Nitzberg [2] has employed exponential smoothing, resulting in reducing the storage requirement by a factor of M.

In this paper, we extend the detection analysis to the clutter map CFAR detector that employs M-pulse noncoherent integration.

This paper is organized as follows. Following this Introduction, the basic assumptions and model description are given in Section II. The clutter map CFAR detector with noncoherent integration is also analyzed in Section II. In Section III, we present and discuss the analytical results. Finally, Conclusions are made in Section IV.

II. Clutter Map CFAR Detector

The output from a radar receiver may be viewed as a random process and the samples of this process as random variables that are characterized by their *probability density function* (pdf). In order to decide if a target signal is present, a test of statistical hypotheses uses pdf of the signal-plus-clutter-plus-noise, H_1, and that of clutter-plus-noise alone, H_0.

A decision of the hypothesis test is made in favor of H_0 or H_1 according to whether

$$Y_n(k) \underset{H_0}{\overset{H_1}{\gtrless}} T\hat{Z}_{n-1}(k) \qquad (1)$$

where $Y_n(k)$ is the *test under cell* (CUT) at the k-th range cell, T is a threshold coefficient to achieve a desired false alarm probability, and $\hat{Z}_{n-1}(k)$ is the estimate of background level. Therefore the detection probability, given the desired false alarm rate, is obtained as

$$P_d = \int_0^\infty f(\hat{z}_{n-1}) \int_{T\hat{Z}_{n-1}}^\infty p_1(y_n)\, dy_n \; d\hat{z}_{n-1} \qquad (2)$$

and the false alarm probability is given by

$$P_{fa} = \int_0^\infty f(\hat{z}_{n-1}) \int_{T\hat{Z}_{n-1}}^\infty p_0(y_n)\, dy_n \; d\hat{z}_{n-1} \qquad (3)$$

where $p_j(y_n)$ (j=0,1) is pdf of the test statistic $Y_n(k)$ for the presence (j=1) and the absence (j=0) of a target, respectively, and $f(\hat{z}_{n-1})$ is pdf of the random variable $\hat{Z}_{n-1}(k)$. By using both the *moment generating function* (mgf) and the contour integration, the detection and the false alarm probabilities can be obtained as follows [3]:

$$P_{fa} = -\sum_{k0} res\left[M_0(s) \frac{M_{\hat{Z}_{n-1}}(-Ts)}{s}, \; s_{k0} \right] \qquad (4)$$

$$P_d = -\sum_{k1} res\left[M_1(s) \frac{M_{\hat{Z}_{n-1}}(-Ts)}{s}, \; s_{k1} \right] \qquad (5)$$

where $M_j(s)$ (j=0,1) is mgf for $p_j(y)$, and s_{k0} (k0 =1,2,...) and s_{k1} (k1 =1,2,...) are the poles of $M_0(s)$ and $M_1(s)$ lying in the left half plane, respectively. $M_{\hat{Z}_{n-1}}(-Ts)$ is obtained by replacing s by $-Ts$ in the mgf of the pdf $f(\hat{z}_{n-1})$ of $\hat{Z}_{n-1}(k)$ and *res* [.] denotes the residue.

A block diagram of the clutter map CFAR detector with noncoherent integration is shown in Fig. 1. The symbol denoted by Z^{-1} means the delay between scans. If $\hat{Z}_{n-1}(k)$ is the (n-1)th estimate of background level and $Y_n(k)$ is the current input data from the k-th cell, then the n-th estimate of background level is given by

$$\hat{Z}_n(k) = (1 - W)\,\hat{Z}_{n-1}(k) \;+\; W\,Y_n(k). \qquad (6)$$

Then, this estimate is multiplied by a threshold coefficient T to yield the adaptive threshold against which the output of CUT at the next time will be compared.

1. Basic assumptions and model description

If we assume that the probability distribution of the clutter-plus-noise level is Rayleigh, the output of the square-law detector has the exponential distribution

$$f(x) = \begin{cases} \dfrac{1}{\beta} Exp\left(-\dfrac{x}{\beta}\right), & x > 0 \\ 0, & otherwise. \end{cases} \qquad (7)$$

The exponential density is a special case of the gamma density with $\alpha = 1$ in the pdf

$$f(x) = \frac{x^{\alpha-1} Exp\left(-\dfrac{x}{\beta}\right)}{\Gamma(\alpha)\beta^{\alpha}}, \quad x \geq 0,\ \alpha \geq 0,\ \beta \geq 0 \qquad (8)$$

where $\Gamma(\alpha)$ denotes the usual gamma function and α is an integer and it can be represented as follows.

$$X_i \;\sim\; G(1, \beta_i) \qquad (9)$$

Since the noncoherent integration is done by summing *M independent and identically distributed* (iid) samples from the square-law detector, pdf at the output of the integrator, Y_i, is the gamma distribution with $\alpha = M$, i.e.,

$$Y_i \;\sim\; G(M, \beta_i) \qquad (10)$$

As the typical statistical model of a target, we use the chi-square family of distribution for a fluctuating target. Swerling target models are well known for the radar detection. They are classified by two kinds of pdf's (statistical distribution) and two kinds of fluctuation rates (correlation properties of target radar cross section), yielding four combinations. When the target signal is constructed from many independently positioned scatterers,

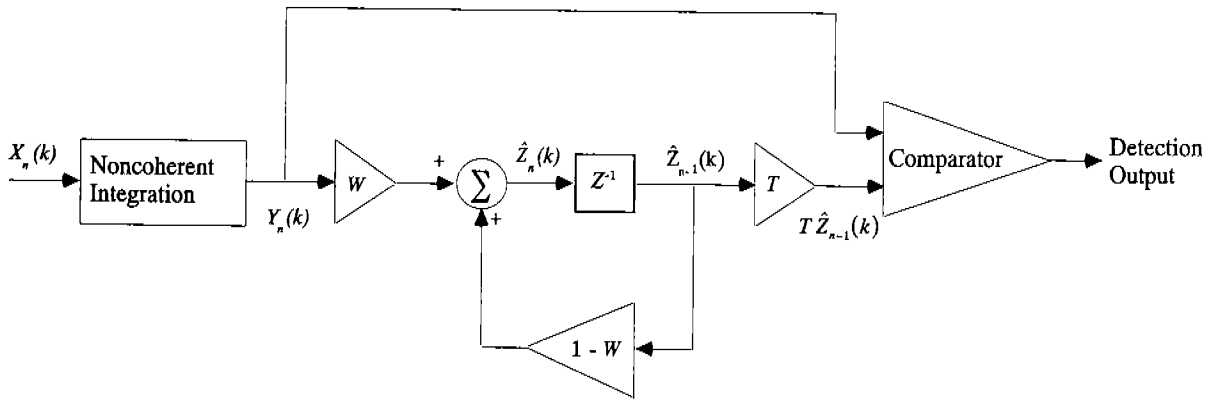

Fig. 1. Block diagram of the clutter map CFAR detector with noncoherent integration.

the pdf of its *radar cross section* (RCS) may be described by a Rayleigh pdf of amplitudes. Also, when the reflected signal contains one dominant constant component in addition to a Rayleigh distributed random component, it can be described by the chi-square pdf with four degrees of freedom. On the other hand, as far as fluctuations are concerned, there are two cases. The first case is scan-to-scan fluctuating target, i.e., there is a complete correlation ($\rho = 1$) between the returned pulses in one scan. The second case is pulse-to-pulse fluctuating target, i.e., there is a complete decorrelation ($\rho = 0$) between the returned pulses.

According to the conditions mentioned so far, the four Swerling target models are defined as follows. Swerling case I and II models apply to fluctuating targets that the amplitude of RCS is a single Rayleigh distributed, independent random variable. Returns from complex targets such as large aircraft are considered to meet this criterion. The distinction between case I and case II is based on the correlation property of a target. Swerling case I is fluctuating with a scan-to-scan basis, i.e., the reflected target returns are constant during the time they are observed in one scan, but fluctuation between scans is randomly occurred. Swerling case II assumes a pulse-to-pulse fluctuating target. On the other hand, Swerling case III and IV models apply to fluctuating targets that the amplitude (RCS) of each pulse in the train is one dominant constant component in addition to a Rayleigh distributed random variable. Returns such as missiles and rockets are considered to meet this criterion. Swerling case III model assumes a scan-to-scan fluctuating target like Swerling I case while Swerling IV target model assumes a pulse-to-pulse fluctuating target like Swerling II case.

The pdf of random variable S which is SNR of the single pulse at the input of the detector is given by

$$p(S) = \frac{1}{\Gamma(K)}\left(\frac{K}{\bar{S}}\right)^{K} S^{K-1} Exp\left(-\frac{KS}{\bar{S}}\right), \quad S > 0 \tag{11}$$

where $\bar{S}$ is the average of S and $K > 0$ is a fluctuation parameter. K represents the degree of freedom. K=1, M, 2, 2M, and ∞ correspond to Swerling cases I, II, III, IV, and the nonfluctuation case, respectively.

The mgf for the chi-square family of fluctuating targets becomes

$$M_j(s) = \int_0^{\infty} M_j(s|S)\, p(S)\ \ dS = \frac{(1+s)^{K-M}}{\left[1 + s\left(1 + \frac{M\bar{S}}{K}\right)\right]^{K}} \tag{12}$$

and

$$M_j(s|S) = (1+s)^{-M}\ \ Exp\left(-\frac{MS}{(1+s)}s\right). \tag{13}$$

(13) is mgf of the statistic Y in the presence of a nonfluctuating target.

2. Analysis of the clutter map CFAR detector

In order to obtain the performance formulas for detection and false alarm probabilities, the mgf of the estimate of background level is required from (4) and (5). The mgf of the clutter estimate is obtained as

$$M_{\hat{Z}_{n-1}}(s) = E_{\hat{Z}_{n-1}}\left[Exp\left(-s\hat{Z}_{n-1}\right)\right]$$

$$= E_Y\left[Exp\left(-sW\sum_{i=0}^{\infty}(1-W)^i\ Y_{n-1-i}\right)\right]$$

$$= \int_0^{\infty} Exp(-sWy_{n-1})\frac{y_{n-1}^{M-1}\left[Exp\left(-\frac{y_{n-1}}{\beta}\right)\right]}{\Gamma(M)\beta^M}\, dy_{n-1}\times\cdots$$

$$\times \int_0^{\infty} Exp\left(-sW(1-W)^i y_{n-1-i}\right)$$

$$\frac{y_{n-1-i}^{M-1}\left[Exp\left(-\frac{y_{n-1-i}}{\beta}\right)\right]}{\Gamma(M)\beta^M}\, dy_{n-1-i}\times\cdots$$

$$= \prod_{i=1}^{\infty}\frac{1}{\left[1+sW(1-W)^{i-1}\beta\right]^M} \qquad (14)$$

where $\beta = 1 + C$ and C is CNR of the k-th cell.

The false alarm probability is obtained from (4), (12), and (14) as follows:

$$P_{fa} = \lim_{l\to\infty}\sum_{q_1=0}^{M-1}\sum_{q_2=0}^{q_1}\cdots\sum_{q_l=0}^{q_{l-1}}\prod_{i=1}^{l}\binom{M+q_i-q_{i+1}-1}{M-1}$$

$$\times\left(\frac{\left[TW(1-W)^{i-1}\beta\right]^{q_i-q_{i+1}}}{\left[1+TW(1-W)^{i-1}\beta\right]^{M+q_i-q_{i+1}}}\right) \qquad (15)$$

where $q_{l+1} = 0$. If we set the number of noncoherent integration to one, i.e., M=1, then (15) becomes

$$P_{fa} = \prod_{i=1}^{\infty}\frac{1}{\left[1+TW(1-W)^{i-1}\beta\right]}. \qquad (16)$$

(16) corresponds to the equation of the false alarm probability for the clutter map CFAR detector in case of single pulse processing obtained by Nitzberg [2].

The detection probability can be obtained under following two conditions. When $1 \le K < M$, (12) has two poles. One of them is the $(M\text{-}K)$th order pole at $s_1 = -1$ and the other is the Kth order pole at $s_2 = -F$, where $F = 1 / (1 + M\bar{S} / K)$. In this case, the detection probability is given by

$$P_d = \lim_{l\to\infty}\sum_{m=0}^{M-K-1}\sum_{q_1=0}^{m}\sum_{q_2=0}^{q_1}\cdots\sum_{q_l=0}^{q_{l-1}}\binom{M-m-2}{K-1}$$

$$\frac{(-F)^K}{G^{M-m-1}}\times\prod_{i=1}^{l}\binom{M+q_i-q_{i+1}-1}{M-1}$$

$$\frac{\left[TW(1-W)^{i-1}\beta\right]^{q_i-q_{i+1}}}{\left[1+TW(1-W)^{i-1}\beta\right]^{M+q_i-q_{i+1}}}$$

$$+\lim_{l\to\infty}\sum_{q=0}^{K-1}\sum_{q_1=0}^{q}\sum_{q_2=0}^{q_1}\cdots\sum_{q_l=0}^{q_{l-1}}(-1)^{q_1}\ \frac{(-F)^{K+q_1-q-1}}{G^{M-q-1}}$$

$$\binom{M-q-2}{M-K-1}\times\prod_{i=1}^{l}\binom{M+q_i-q_{i+1}-1}{M-1}$$

$$\frac{\left[TW(1-W)^{i-1}\beta\right]^{q_i-q_{i+1}}}{\left[1+TFW(1-W)^{i-1}\beta\right]^{M+q_i-q_{i+1}}} \qquad (17)$$

where G=1-F.

When $1 \le M \le K$, since (12) has the Kth order pole at $s=-F$, the detection probability is obtained from (5), (12), and (14) as follows:

$$P_d = \lim_{l\to\infty} \sum_{m=M-1}^{K-1} \sum_{q_1=0}^{m} \sum_{q_2=0}^{q_1} \cdots \sum_{q_l=0}^{q_{l-1}} \binom{K-M}{K-m-1} \frac{F^{K+q_1-m-1}}{G^{M-m-1}} \times \prod_{i=1}^{l} \binom{M+q_i-q_{i+1}-1}{M-1} \frac{\left[TW(1-W)^{i-1}\beta\right]^{q_i-q_{i+1}}}{\left[1+TFW(1-W)^{i-1}\beta\right]^{M+q_i-q_{i+1}}} \quad (18)$$

If we set both the number of noncoherent integration and the value of the fluctuation parameter to one, i.e., $M=K=1$, then (18) becomes

$$P_d = \prod_{i=1}^{\infty} \frac{1}{\left[1+TFW(1-W)^{i-1}\beta\right]} = \prod_{i=1}^{\infty} \frac{1}{\left[1+T\frac{\beta}{1+\bar{S}}W(1-W)^{i-1}\right]} \quad (19)$$

which reduces to the equation of the detection probability for single pulse detection derived in [2].

III. Analytical Results and Discussion

In this section, we obtain the performance of the clutter map CFAR detector. We first show detection performances of a Swerling II target for different number of integrated pulses and then show detection performances of clutter map CFAR detector for four types of Swerling target models.

1. Detection performance for a Swerling II target

Frequency diversity technique can make it possible to obtain decorrelated target returns even though it requires additional system complexity. Thus, Swerling II target model is important because its target returns can be obtained practically by using frequency diversity. In this Section, we analyze the performance of the Swerling II model, i.e., $K = M$. Parameters to implement clutter map CFAR detector are given in Table 1.

Table 1

Threshold Coefficients (T) for Various Weight Value and Different Number of Integrated Pulses (l = 70, $P_{fa} = 10^{-6}$)

M	W		
	0.1	0.2	0.3
1	19.328	26.759	32.276
2	10.153	12.359	15.168
3	7.368	8.532	9.958

Fig. 2 shows the detection performance as a function of target SNR for different number of integrated pulses (M = 1, 2). From the figure, one can see that the detection performance of clutter

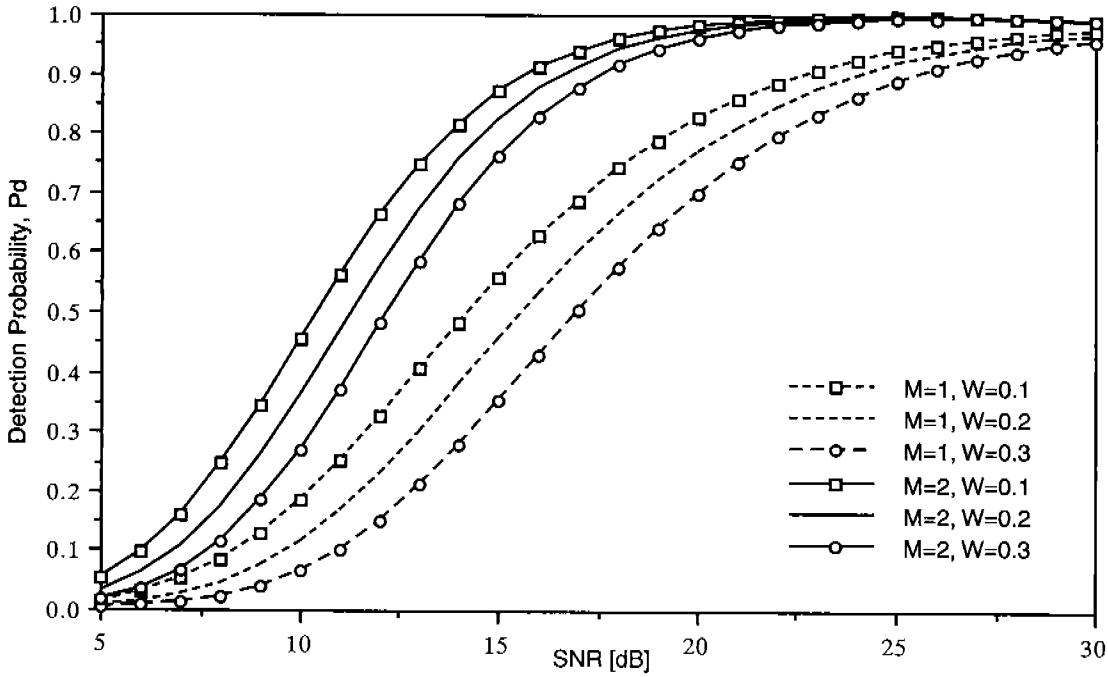

Fig. 2. Detection probabilities vs. target SNR for Swerling II target.

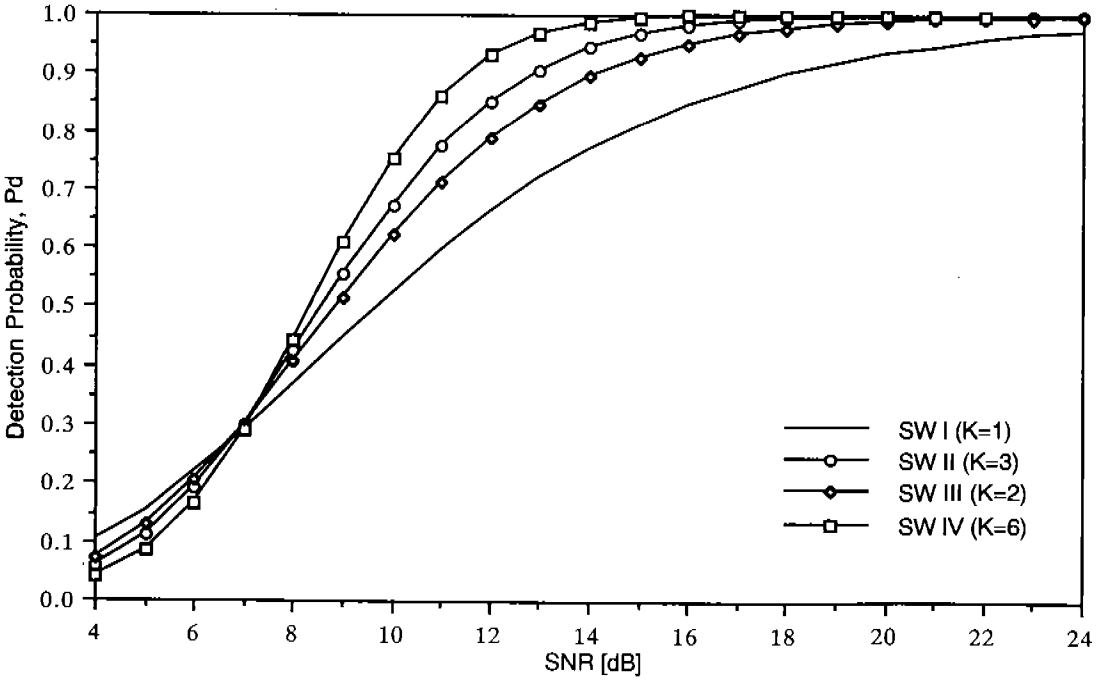

Fig. 3. Detection probabilities vs. target SNR for clutter map CFAR detector of Swerling targets (W=0.1, M=3).

map CFAR detector for $M = 2$ is superior to that for $M = 1$. We can also see that the lower the weight value, the higher the detection probability.

2. Detection performance for four Swerling target models

In this experiment, we set $M = 3$ and $W = 0.1$. Thus, K for Swerling cases I, II, III, and IV is 1, 3, 2, and 6, respectively.

Detection performance as a function of per-pulse target SNR is shown in Fig. 3. In the figure, the curve with square symbols represents the detection performance for a Swerling IV target and the plain solid curve a Swerling I target. The Swerling I and III target models correspond to complete correlation ($\rho = 1$). Also, the Swerling II and IV target models correspond to complete decorrelation ($\rho = 0$). From the figure, we can see that the the detection performance of the completely decorrelated target signal is better than that of the completely correlated target. By the property of (12), detection performance of the correlated target signal is between two extreme cases. It can be shown that for about $P_d > 0.3$, the more the correlation, the higher single pulse SNR is required to achieve a given detection probability, i.e., more fluctuation loss. Also, one can see that when the detection probability is low (in this case, about 0.3), the more the fluctuations of target returns, the more the SNR gain. This is the reason that a few target returns, which is greater than the average value, improve the detection probability when the average SNR is low [4]. So, there may exist crossing in Fig. 3. In order to reduce the effect of the target fluctuation, one may adopt the pulse-to-pulse waveform diversity to decorrelate the M signal returns.

IV. Conclusions

In this paper, we analyze the performance of the clutter map CFAR detector that employs M-pulse noncoherent integration. Performance formulas for both the false alarm and the detection probabilities are derived.

The analytical results show that the larger the number of integrated pulses, the higher the detection probability. It also is shown that the lower the weight value, the higher the detection probability when we use the same number of integrated pulses. On the other hand, the analytical results for Swerling target models show that the the detection performance of the completely decorrelated target signal is better than that of the completely correlated target.

References

[1] H. M. Finn and R. S. Johnson, "Adaptive detection mode with threshold control as a function of spatial sampled clutter level estimates," *RCA review*, 29, Sept. 1968, pp. 414-464.

[2] R. Nitzberg, "Clutter Map CFAR Analysis," *IEEE Transactions on Aerospace and Electronics Systems*, AES-22, 1986, pp. 419-421.

[3] X. Y. Hou, N. Morinaga and T. Namekawa, "Direct Evaluation of Radar Detection Probabilities," *IEEE Transactions on Aerospace and Electronic Systems*, AES-23, July 1987, pp. 418-424.

[4] N. Levanon, Radar Principles, John Wiley & Sons: New-York, 1988.

Chang-Joo Kim was born in Kongju, on December 21, 1956. He received the B. S. degree in electronics engineering from Hankuk Aviation University in 1980, and the M.S. and Ph. D. degrees in electrical engineering from the KAIST, in 1988 and 1993, respectively.

From 1980 to 1982 he was engaged as a research engineer at ADD. Since 1983 he has been with the communication fields of ETRI, where he is now a senior research engineer in the radio signal processing section. His current interests involves signal detection, channel coding, and digital signal processing.

Hyuck-Jae Lee was born in Inchon, on November 20, 1947. He received the B. S. degree in electronics engineering from Seoul National University, in 1970, and the Ph. D. degree in electrical engineering from Oregon State University in 1982 majored in electromagnetic fields and microwave engineering.

Since 1983 he joined the radio communication laboratory of ETRI, and has been working on the fields of radio signal processing, radio monitoring and automation, digital mobile communication, and radio wave utilization projects. Dr. Lee is now a director of radio technology department.